

Biophysical properties of heterotypic gap junctions newly formed between two types of insect cells

Feliksas F. Bukauskas, Rolf Vogel and Robert Weingart*

Department of Physiology, University of Bern, B hlplatz 5, CH-3012 Bern, Switzerland

1. Cell pairs of the insect cell line Sf9 (*Spodoptera frugiperda*) were chosen to examine the electrical properties of gap junction channels. The dual voltage-clamp method was used to control the membrane potential of each cell ($V_{m,1}$ and $V_{m,2}$) and hence the junctional voltage gradient (V_j), and to measure intercellular current.
2. Studies with preformed pairs revealed that the gap junction conductance (g_j) is controlled by a V_j - and a V_m -sensitive gate. At steady state, $g_j = f(V_j)$ was bell shaped and symmetrical (Boltzmann: $V_{j,0} = -54$ and 55 mV, the normalized minimum conductance at large V_j values ($g_{j,min}$) = 0.24 and 0.23 , $z = 5.5$ and 6.1 for negative and positive V_j , respectively) and $g_j = f(V_m)$ was S shaped ($V_{m,0} = 13$ mV, $g_{j,min} = 0$, $z = 1.5$).
3. Single channels exhibited two conductances, a main state ($\gamma_{j,main}$) of 224 pS and a residual state ($\gamma_{j,residual}$) of 42 pS.
4. We conclude that gap junctions in Sf9 cells behave similarly to those in the insect cell line C6/36 (*Aedes albopictus*).
5. An induced cell pair approach was used to examine heterotypic gap junction channels between Sf9 cells and C3/36 cells.
6. Heterotypic channels showed a $\gamma_{j,main}$ of 303 pS and a $\gamma_{j,residual}$ of 45 and 64 pS, depending on whether the Sf9 cell or C6/36 cell was positive inside.
7. In heterotypic gap junctions, $g_j = f(V_j)$ was bell shaped and asymmetrical (g_j was more sensitive to V_j when the C6/36 cell was positive inside) and $g_j = f(V_m)$ was S shaped ($V_{m,0} = 2$ mV, $g_{j,min} = 0$, $z = 2.9$).
8. We conclude that heterotypic channels possess a V_j - and V_m -sensitive gating mechanism. V_j gating involves two gates, one located in each hemi-channel. V_j gates are operated independently and close when the cytoplasmic aspect is made positive.
9. A comparison of homo- and heterotypic channel data suggests that docking of hemi-channels may affect channel gating, but not channel conductance.

Gap junctions allow intercellular communication via current flow or exchange of molecules. This concept of cellular co-ordination is exploited by various tissues in different animal species. Gap junctions are aggregates of channels. Each channel consists of two hemi-channels (connexons) located in the membranes of adjacent cells; each connexon accommodates six proteins (connexins) forming an aqueous pore (see Bennett, Barrio, Bargiello, Spray, Hertzberg & Saez, 1991). The analysis of amino acid sequences suggests that connexins traverse the lipid bilayer four times, thus creating four transmembrane domains, two extracellular loops, one intracellular loop, and a cytoplasmic amino- and carboxy-terminus (see Beyer, 1993). This picture has emerged from studies on vertebrate cells. So far, cDNAs of sixteen connexins have been cloned and sequenced (see

Beyer, 1993). The properties of several channels have been determined at the macroscopic and microscopic current level (see Waltzman & Spray, 1995). The elucidation of structure–function relationships is underway in some cases. In contrast, only little is known about gap junction channels in other classes of the animal kingdom. For example, in arthropods virtually no information is available on structure (Berdan & Gilula, 1988). Despite extensive homology searches, no gap junction protein could be identified as yet (but see Barnes, 1994). Furthermore, there is no functional evidence for the existence of different types of channels in arthropods (Verselis, Bennett & Bargiello, 1991; Bukauskas, Kempf & Weingart, 1992a; Churchill & Caveney, 1993; Bukauskas & Weingart, 1994a).

* To whom correspondence should be addressed.

Experiments on cell pairs have shown that insect gap junctions possess two voltage-sensitive gates, one controlled by the junctional voltage gradient (V_j), the other one by the membrane potential (V_m) (Obaid, Socolar & Rose, 1983; Verselis *et al.* 1991; Bukauskas *et al.* 1992a; Churchill & Caveney, 1993). To study the electrical properties of gap junction channels, we have previously used an insect cell line (C6/36; from the mosquito *Aedes albopictus*) in conjunction with the dual voltage-clamp method (Bukauskas *et al.* 1992a; Bukauskas & Weingart, 1994a). We have now extended these studies examining another insect cell line (Sf9; from the fall armyworm *Spodoptera frugiperda*). The junctional currents turned out to be different in Sf9 cells and C6/36 cells, suggesting that these cells express different gap junction proteins.

We were also interested to see if Sf9 cells and C3/36 cells form heterotypic gap junction channels. Such channels made of vertebrate connexins were observed in native cell lines (e.g. Werner, Levine, Rabadan-Diehl & Dahl, 1989; Nicholson *et al.* 1993) as well as in *Xenopus* oocytes and cell lines after expression of connexin cDNA (e.g. Barrio *et al.* 1991; Rubin, Verselis, Bennett & Bargiello, 1992; White, Bruzzone, Wolfram, Paul & Goodenough, 1993; Bukauskas, Elfgang, Willecke & Weingart, 1995a; Moreno, Fishman, Beyer & Spray, 1995). Examination of mixed channels may lead to information on docking of hemi-channels and polarity of V_j gating. Of particular interest are channels with hemi-channels of widely different properties. They may elucidate the behaviour of single hemi-channels (Bukauskas *et al.* 1995a; Weingart, Bukauskas, Valiunas, Vogel, Willecke & Elfgang, 1996). To study Sf9–C6/36 channels, we have used an induced cell pair approach (see Bukauskas & Weingart, 1994a). This method allowed us to examine microscopic (single channels) and macroscopic currents (many channels) in the same preparation. Preliminary data have been published before (Bukauskas & Weingart, 1994b).

METHODS

Cells

Two types of insect cells have been used, Sf9 cells (derived from pupal ovaries of the fall armyworm *Spodoptera frugiperda*; American Tissue Type Culture Collection code CRL 1711; Smith *et al.* 1985) and C6/36 cells (derived from larvae of the mosquito *Aedes albopictus*; ATCC code CRL 1660; Igarashi, 1978). Sf9 cells were grown at 27 °C in Grace medium (50% Grace 1, 50% Grace 2; code 47308; Serva, Wallisellen, Switzerland) containing 100 U ml⁻¹ penicillin, 100 µg ml⁻¹ streptomycin (code 2212 Seromed; Fakola, Basel, Switzerland) and 250 µg ml⁻¹ amphotericin B (code 47982; Serva). Grace 2 contained 20% fetal calf serum, 3.33 mg ml⁻¹ yeastolate (code 5577-15-5; Difco Laboratories, Detroit, MI, USA) and 3.33 mg ml⁻¹ lactalbumin (code 5996-01; Difco Laboratories). The cells were passaged weekly and diluted 1:8 (with the above medium). For the experiments, monolayers of cells were harvested and resuspended in Grace 1. Thereafter, the cells were plated onto sterile glass coverslips placed in multiwell culture dishes (1 ml per well). After 1 h, 1 ml Grace 2 was added to each well (final cell

density, ~10⁴ cells cm⁻²). C6/36 cells were grown at 28 °C in RPMI 1640 medium (Gibco, Paisley, UK) containing 20% fetal calf serum, 100 U ml⁻¹ penicillin and 100 µg ml⁻¹ streptomycin (code 2212, Biochrom, Berlin, Germany). The cells were passaged weekly and diluted 1:10 with the above medium. For the experiments, monolayers of cells were harvested and resuspended in RPMI 1640 medium containing 20% fetal calf serum. Subsequently the cells were seeded at a density of ~10⁴ cells cm⁻² onto sterile glass coverslips placed in multiwell culture dishes. Electrophysiological measurements were carried out 1–3 days after plating.

Solutions and pipettes

The experiments were performed in modified Krebs–Ringer solution (mM): NaCl, 140; KCl, 4; CaCl₂, 2; MgCl₂, 1; Hepes, 5 (pH 7.4); glucose, 5; pyruvate, 2. Patch pipettes were pulled from glass capillaries (GC150TF-10; Clark Electromedical Instruments, Pangbourne, Berks, UK) with a horizontal puller (DMZ; Zeitz Instruments, Augsburg, Germany). The pipettes were filled with pipette solution (mM): NaCl, 10; potassium aspartate, 120; CaCl₂, 1; MgCl₂, 1; MgATP, 3; Hepes, 5 (pH 7.2); EGTA, 10 (pCa ~8); filtered through 0.22 µm pores. The filled pipettes had DC resistances of 3–5 MΩ (tip size, ~1 µm).

Electrical measurements

The experimental chamber consisted of a Perspex frame with a glass bottom and was mounted on the stage of an inverted microscope equipped with phase-contrast optics (Diaphot-TMD, Nikon; Nippon Kogaku, Tokyo, Japan). The chamber was perfused with Krebs–Ringer solution at room temperature (22–25 °C) by means of gravity (bath volume, 1 ml; flow rate, 1–2 ml min⁻¹). To study the electrical properties of gap junction channels, we used a dual voltage-clamp method (Bukauskas *et al.* 1992a). Experiments were carried out on two types of preparations, preformed cell pairs (Bukauskas & Weingart, 1992a) and induced cell pairs (Bukauskas & Weingart, 1994a). In the latter case, two single cells in close proximity were selected visually. Each cell was then brought into contact with a patch pipette connected to a separate amplifier (EPC-7; List Electronic, Darmstadt, Germany). After establishment of the whole-cell, tight-seal recording conditions, the cells were pushed against each other by moving the patch pipettes via hydraulic micromanipulators (WR-88; Narishige Scientific Instruments, Tokyo, Japan). This approach allows one to control the membrane potential of each cell (V_1 and V_2) individually and to monitor the associated current through pipette 1 (I_1) and pipette 2 (I_2) separately. In the case of two separate cells, I_1 and I_2 reflect the current through the membrane of cell 1 ($I_{m,1}$) and cell 2 ($I_{m,2}$), respectively. In the case of a functional cell pair, I_1 and I_2 represent the sum of two currents, $I_{m,1} + I_j$ and $I_{m,2} - I_j$, respectively, where I_j is the current through the gap junction. Deflections in I_1 and I_2 , coincident in time and opposite in polarity, correspond to changes in I_j . The conductance of a gap junction channel was determined as $\gamma_j = I_j / (V_2 - V_1)$. The difference $V_2 - V_1$ corresponds to the voltage gradient across the gap junction, V_j .

Signal recording and analysis

Voltage and current signals were recorded on FM tape (SE3000; SELab, Feltham, UK) at between 3 and 3–4 in s⁻¹ (DC bandwidth, 2.5 kHz). For off-line analysis with a personal computer, the current signals were filtered at 1 kHz (–3 dB) using an 8-pole Bessel filter (902LPPF; Frequency Devices, Haverhill, MA, USA) and digitized at 3.33 kHz with a 12-bit analog-to-digital converter (IDA 12120; INDEC Systems, Capitola, CA, USA). Data analysis was performed with the acquisition system C-Lab (INDEC

Systems). Measurements of membrane potentials were corrected for the liquid junction potential between the pipette solution and bath solution (-12 mV). Results are presented as means \pm 1 s.e.m. Curve fitting was performed with SigmaPlot (Jandel Scientific, Erkrath, Germany).

RESULTS

Dependence of g_j on junctional potential

First we have examined the sensitivity of junctional currents, I_j , on junctional voltage gradients, V_j , using preformed pairs of Sf9 cells. Figure 1A illustrates the voltage-clamp protocol adopted. Long-lasting voltage pulses of different fixed amplitudes were administered to cell 2 every 10–40 s (trace V_2). A depolarizing pulse of 25 mV gave rise to a constant I_j (trace I_1 , left-hand side). A V_j pulse of 50 mV revealed an I_j with a marginal time-dependent decay (middle). A 75 mV pulse was accompanied by an I_j with pronounced time-dependent relaxation (right-hand side), i.e. the instantaneous current, $I_{j,\text{inst}}$, was followed by a monotonic decay to a new steady state, $I_{j,\text{ss}}$. A comparison of the I_j records indicates that the current noise increased with increasing V_j . This suggests an increase in single-channel activity. Hyperpolarizing test pulses (25 mV, 200 ms) were administered intermittently to cell 2 (downward deflections in trace V_2) to monitor the electrical stability of the preparation.

Figure 1B summarizes the analysis of six complete experiments. For each V_j examined, the amplitudes of the $I_{j,\text{inst}}$ and $I_{j,\text{ss}}$ were determined and the instantaneous and steady-state conductances, $g_{j,\text{inst}}$ and $g_{j,\text{ss}}$, respectively, were calculated. Individual values of $g_{j,\text{ss}}$ were normalized with respect to $g_{j,\text{inst}}$ ($g_{j,\text{norm}} = g_{j,\text{ss}}/g_{j,\text{inst}}$) and plotted *versus* V_j . The data points follow a symmetrical bell-shaped distribution which fails to reach zero conductance at large V_j values. The continuous curve represents the best fit of the

data to a two-state Boltzmann process given by the following equation:

$$g_{j,\text{norm}} = \{ (1 - g_{j,\text{min}}) / [1 + \exp(A(V_j - V_{j,0}))] \} + g_{j,\text{min}}, \quad (1)$$

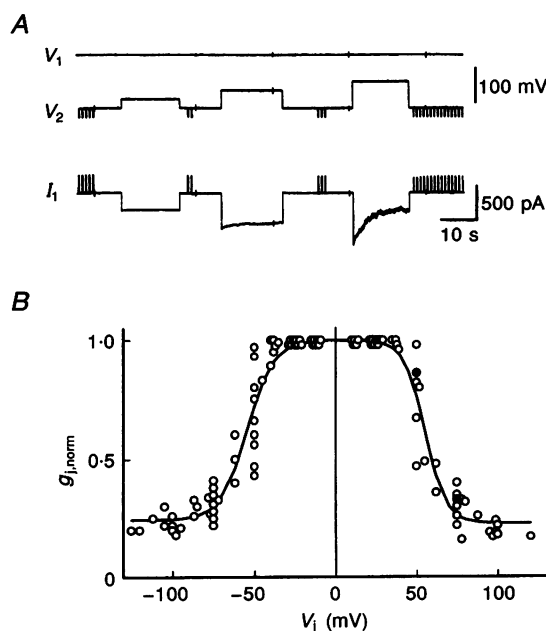
where $V_{j,0}$ corresponds to V_j at which g_j is half-maximally inactivated and $g_{j,\text{min}}$ is the normalized minimal conductance at large V_j values. A is a constant expressing gating charge, $zq(kT)^{-1}$, where z corresponds to the number of equivalent gating charges moving through the entire electric field applied, q is the electron charge, and k and T represent the Boltzmann constant and the temperature in kelvins, respectively. The analysis yielded a $V_{j,0}$ of -54 and 55 mV, a $g_{j,\text{min}}$ of 0.24 and 0.23 , and a z of 5.5 and 6.1 for negative and positive values of V_j , respectively. In these preparations, $g_{j,\text{inst}}$ averaged 5.8 ± 1.4 nS. In three out of nine cell pairs, I_j was insensitive to V_j and 3 mM heptanol. This suggests that the intercellular current flow was by means of cytoplasmic bridges rather than gap junctions (Bukauskas *et al.* 1992a, b).

Dependence of g_j on membrane potential

In another series of experiments, we have studied the dependence of I_j on membrane potential (V_m) using preformed pairs of Sf9 cells. Figure 2A illustrates the pulse protocol applied. Both cells of a preparation were clamped to -65 mV. Identical conditioning pulses were then applied concomitantly to cell 1 and cell 2 (traces V_1 and V_2). To assess the associated changes in I_j , small test pulses were administered repetitively to cell 2 (-25 mV, 200 ms, 1 Hz) giving rise to V_j gradients (downward deflections in V_2) and hence intercellular current flow, I_j (upward deflections in I_1). The conditioning pulses lasted 10–40 s, depending on V_m . In each case, I_j was allowed to reach a new steady-state level. Figure 2A shows that depolarization of V_m to 35 and 60 mV produced a time-dependent decrease in I_j . The larger the depolarization, the faster was the speed of I_j decline and

Figure 1. Homotypic gap junctions in preformed pairs of Sf9 cells: dependence of intercellular coupling on gap junction potential (V_j)

A, responses of gap junction currents (I_j) to V_j . Traces illustrate the membrane potential of cell 1 (V_1) and cell 2 (V_2) and the current measured in cell 1 (I_1). Deflections in V_2 and I_1 correspond to V_j and I_j , respectively. An increase in V_j from 25 mV to 50 and 75 mV (upward deflections in V_2) led to the evolution of voltage- and time-dependent changes in I_j (downward deflections in I_1). Short V_j test pulses (downward spikes in V_2) served to monitor the stability of the preparation (upward spikes in I_1). Holding potential, $V_h = -70$ mV. B, plot of normalized gap junction conductance at steady state ($g_{j,\text{norm}}$) *versus* V_j . Data from 6 cell pairs. ● indicate values gained from records in A. The continuous curve is the theoretical fit of data to the Boltzmann equation with $V_{j,0} = -54$ and 55 mV; $g_{j,\text{min}} = 0.24$ and 0.23 ; $z = 5.5$ and 6.1 for negative and positive V_j , respectively.



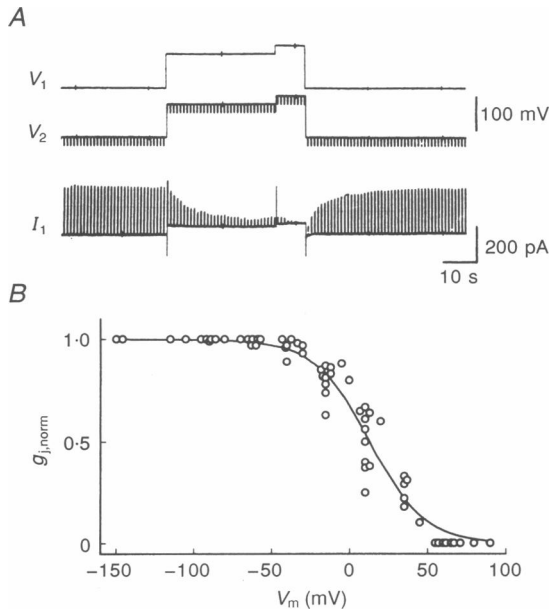


Figure 2. Homotypic gap junctions in preformed pairs of Sf9 cells: dependence of intercellular coupling on membrane potential (V_m)

A, records of V_1 , V_2 and I_1 representing the membrane potential of cell 1 and cell 2 and the current measured in cell 1, respectively. A conditioning pulse was applied simultaneously to both cells to depolarize V_m from -65 mV to 35 and 60 mV. The associated gap junction conductance (g_j) was assayed by repetitive application of a test pulse to cell 2 (-25 mV, 200 ms, 1 Hz) giving rise to a junctional voltage gradient V_j (downward deflections in V_2) and hence a junctional current I_j (upward deflections in I_1). B, plot of normalized gap junction conductance at steady state ($g_{j, \text{norm}}$) versus V_m . Data from 8 preparations. The continuous curve shows the theoretical fit of data to the Boltzmann equation with $V_{m,0} = 13$ mV, $g_{j, \text{min}} = 0$ and $z = 1.5$.

the more pronounced the extent of I_j decrease. At a V_m of 60 mV, I_j was virtually zero at steady state. When V_m was returned to -65 mV, I_j recovered as a function of time. Hyperpolarization of V_m had no effect on I_j (data not shown).

The records in Fig. 2A and others from the same experiment were analysed for g_j prevailing immediately before a conditioning pulse ($g_{j, \text{control}}$) and at the end of a conditioning pulse ($g_{j, \text{ss}}$). Values of $g_{j, \text{ss}}$ were then normalized with respect to $g_{j, \text{control}}$ ($g_{j, \text{norm}} = g_{j, \text{ss}}/g_{j, \text{control}}$) and plotted versus V_m . Figure 2B summarizes the results of eight experiments. The data points describe a sigmoidal curve with $g_{j, \text{norm}}$ altering from unity to zero as V_m is depolarized. Specifically, $g_{j, \text{norm}}$ was constant for values of V_m ranging from -150 mV to approximately -75 mV. It decreased progressively when V_m was depolarized to 0 mV and beyond. At $V_m > 50$ mV, $g_{j, \text{norm}}$ was virtually zero. The continuous curve represents the best fit of the data to the Boltzmann equation (see eqn (1)). For the curve depicted, $V_{m,0}$ was 13 mV, $g_{j, \text{min}}$ was 0 , and z was 1.5 .

Properties of homotypic gap junction channels

Next we determined the properties of single channels formed between Sf9 cells. We made use of preformed cell pairs whose gap junctions consisted of a single channel or several channels. Figure 3 illustrates signals from a preparation with a single operational channel. V_1 and V_2 were clamped to -65 mV. Cell 2 was then pulsed repetitively (± 75 mV, 300 ms, 0.1 Hz) to establish a V_j gradient and hence to induce an I_j . During the V_j pulses I_1 exhibited fast transitions attributable to the operation of a gap junction channel (upper I_1 trace: response to V_2 depolarization; lower I_1 trace: response to V_2 hyperpolarization). I_j fluctuated rapidly between two discrete levels corresponding to the state of a fully open channel and a partially closed channel. During pulse application I_j did not return to zero current (continuous lines), the level prevailing before and after pulsing.

The analysis of such records collected from six preparations is summarized in Fig. 4. Individual I_j signals were assessed for discrete current levels and the conductances, γ_j ,

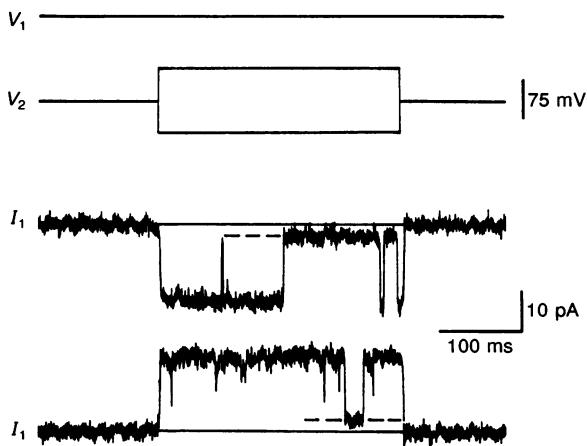
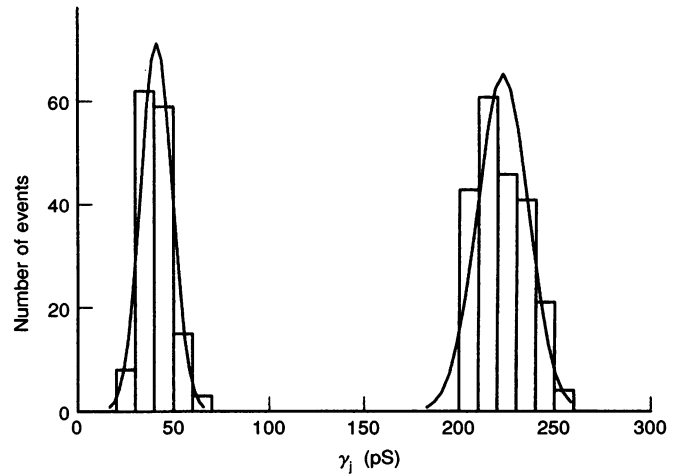


Figure 3. Single-channel activity examined in a preformed pair of Sf9 cells whose gap junction consisted of a single channel

Application of a depolarizing or hyperpolarizing pulse of 75 mV to cell 2 (superimposed V_2 traces) provoked a negative or positive V_j , respectively. The associated junctional currents I_j (deflections in I_1 traces) fluctuated between two discrete levels attributable to the fully open state and residual state of the channel (dashed lines). During the pulse, the current did not return to the reference level (continuous lines). The polarity of V_j had no effect on the current amplitudes. $V_h = -65$ mV.

Figure 4. Histogram of single-channel conductances (γ_j) obtained from preformed pairs of homotypic gap junction channels (Sf9–Sf9)

Data from 6 preparations were pooled in consecutive 10 pS bins. The number of observations was plotted versus γ_j . The continuous curves are the theoretical fits of data to a Gaussian distribution. The left-hand distribution revealed a mean value of 42 ± 8 pS (148 events) and reflects the conductance of the incompletely closed channel, $\gamma_{j,\text{residual}}$. The right-hand distribution yielded a mean value of 224 ± 13 pS (214 events) and corresponds to the conductance of the fully open channel, $\gamma_{j,\text{main}}$.



determined. The data obtained in this way were pooled in 10 pS bins and plotted versus γ_j . The resulting histogram shows two narrow peaks which are completely separated. The left-hand peak yielded a mean value of 42 ± 8 pS ($n = 148$) and is attributable to the conductance of a partially closed channel, $\gamma_{j,\text{residual}}$. The right-hand peak revealed a mean value of 224 ± 13 pS ($n = 214$) and corresponds to the conductance of a fully open channel, $\gamma_{j,\text{main}}$. The ratio $\gamma_{j,\text{main}}/\gamma_{j,\text{residual}}$ was 5.3. When V_m was depolarized progressively from -100 to 25 mV, there was no change in $\gamma_{j,\text{main}}$ or $\gamma_{j,\text{residual}}$ ($V_j = 12$ – 25 mV). However, associated with this intervention, the channels exhibited slow transitions (tens of milliseconds) aimed at the fully closed state (data not shown). As a result, fast channel flickering came to a halt. Hence Sf9–Sf9 channels appear to behave like C6/36–C6/36 channels (Bukauskas & Weingart, 1994a).

Formation of heterotypic gap junction channels between Sf9 cells and C6/36 cells

A comparison of the g_j data indicates that gap junctions of Sf9 cells and C6/36 cells exhibit distinctly different V_j sensitivities (Sf9 cells: $V_{j,0} = -54$ and 55 mV, $g_{j,\text{min}} = 0.24$ and 0.23 , $z = 5.5$ and 6.1 for negative and positive V_j values, respectively (see above); C6/36 cells: $V_{j,0} = -31$ and 24 mV, $g_{j,\text{min}} = 0.15$ and 0.14 , $z = 2.7$ and 3.3 for negative and

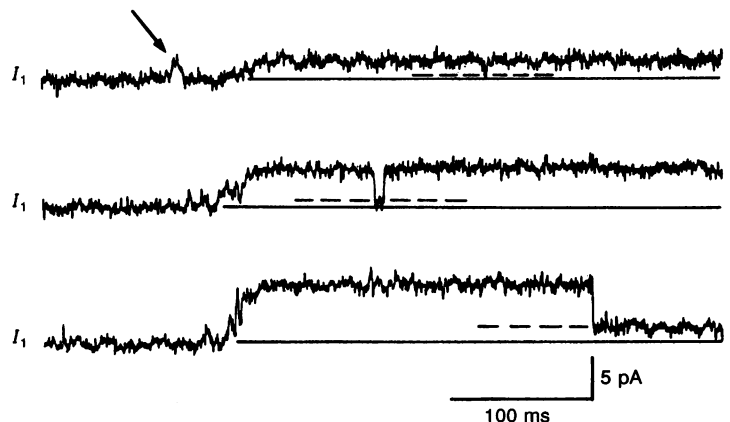
positive V_j values, respectively; Weingart & Bukauskas, 1995). This suggests that the two cell lines express different types of gap junction proteins. This renders it interesting to examine the putative formation of heterotypic gap junction channels between Sf9 cells and C6/36 cells (Sf9–C6/36).

To examine this possibility, Sf9 cells were removed from the substrate by gentle agitation with a Pasteur pipette. A drop of cell suspension was added to the experimental chamber containing a coverslip with adherent C6/36 cells. Based on optical criteria (position of C6/36 cells on coverslip, cell size, cell shape), a Sf9 cell and a C6/36 cell in close proximity were selected for an experiment. Each cell was then attached to a patch pipette, whole-cell recording conditions established for both, and the membrane potential of the two cells clamped to different voltages ($V_1 \neq V_2$). Subsequently the cells were pushed against each other by gently moving the pipettes via micromanipulators. As a result of the physical cell-to-cell contact, formation of gap junction channels occurred after a variable delay giving rise to a stepwise increase in I_1 (not shown).

Figure 5 shows I_1 records obtained from different preparations. Each record documents the first opening of a newly inserted gap junction channel. In these examples, V_j was set to -9 , -15 and -23 mV (top to bottom traces, respectively). All transitions in the I_1 signals were

Figure 5. Formation of heterotypic gap junction channels between a Sf9 cell and a C6/36 cell (Sf9–C6/36)

Examples of the first opening of a newly formed channel recorded at V_j values of 9 , 15 and 23 mV (from top to bottom, respectively). Upward deflections correspond to channel openings. The first channel opening was slow compared with subsequent closings and openings (middle and bottom traces). Continuous lines indicate the zero coupling current, dashed lines are the current level associated with an incompletely closed channel ($\gamma_{j,\text{residual}}$). The arrow shows an unsuccessful attempt to open a channel (top trace).



accompanied by concomitant ones in I_2 of opposite polarity (not shown), hence they correspond to gap junction events. The first transition in each trace was slow and reflects the first opening of a newly formed channel. The slow transitions lasted 44 ± 6 ms ($n = 8$; range, 35–62 ms). The subsequent transitions were fast (< 2 ms) and indicated regular channel gating. During the first transition the contour of I_1 was often discontinuous implying the involvement of discrete current levels (middle and bottom trace). In one example (top trace), the earliest deflection corresponds to an unsuccessful attempt to open a channel (see arrow). Associated with the fast transitions (middle and bottom traces), I_1 jumped between two discrete levels corresponding to the main open state and the residual state (dashed lines). The analysis of these records yielded values for γ_j of approximately 300 pS for the main state and approximately 50 pS for the residual state. Like in the case of homotypic channels between Sf9 cells or C6/36 cells, I_1 did not return to the zero current level (continuous lines) suggesting that the channels failed to close completely.

Examination of I_j signals also provided information about the formation of gap junctions. The average time lag between the incident of cell-to-cell contact and first channel opening was 12.9 ± 2.3 min ($n = 8$). The subsequent insertion of additional channels followed a sigmoidal time course. Steady-state coupling ($g_j = 2.1 \pm 1$ nS) was reached after 15 ± 5 min. During the process of channel formation, there was no current leak between the intra- and extracellular space. This suggests that docking between two hemi-channels is complete before a new channel opens.

Properties of heterotypic gap junction channels

To determine the properties of Sf9–C6/36 channels, we utilized induced cell pairs after the formation of one or two channels. Figure 6A shows a scheme representing the cellular arrangement. The records in Fig. 6B were gained from a preparation with a single gap junction channel.

Initially, V_1 and V_2 were clamped to -85 and -60 mV, respectively, to establish a V_j of 25 mV ($V_j = V_2 - V_1$; inside of the C6/36 cell positive with respect to the Sf9 cell). Under this condition I_2 revealed a net outward current attributable to junctional current flow. The continuous line refers to zero current. I_2 rapidly fluctuated between two discrete levels corresponding to the main state and the residual state (channel opening: upward deflections). The analysis indicated that the time spent in the two states was similar ($V_j = 25$ mV; open channel probability (P_o), ~ 0.6). V_1 was abruptly depolarized from -85 to -60 mV and, a few milliseconds later, to -35 mV while V_2 was maintained. This provoked an inversion of the V_j polarity (inside of the Sf9 cell positive with respect to the C6/36 cell) without altering the driving force for junctional currents. Under this condition I_2 exhibited a net inward current caused by gap junction channel events. Again, I_2 fluctuated rapidly between two discrete levels corresponding to the main state and the residual state (channel opening: downward deflections). However, now the channel spent most of the time in the main state ($V_j = -25$ mV; P_o , ~ 0.95). This suggests that the activity of heterotypic channels is dependent on the polarity of V_j .

Figure 6C shows similar findings obtained from a cell pair with two gap junction channels. In this case the pulse protocol was inverted: a V_j gradient of -25 mV (inside of the Sf9 cell positive with respect to the C6/36 cell) was flipped to 25 mV (inside of the C6/36 cell positive with respect to the Sf9 cell). As a result, during the first half of the protocol, the channels mainly stayed in their main state (trace I_2). On rare occasions I_j decreased to a level corresponding to $\gamma_{j,\text{main}} + \gamma_{j,\text{residual}}$, but never to a level equivalent to $2\gamma_{j,\text{residual}}$. During the second half of the protocol, the channels were partially in the main state and partially in the residual state. Hence I_j resided at a level corresponding to $2\gamma_{j,\text{main}}$, $\gamma_{j,\text{main}} + \gamma_{j,\text{residual}}$, or $2\gamma_{j,\text{residual}}$.

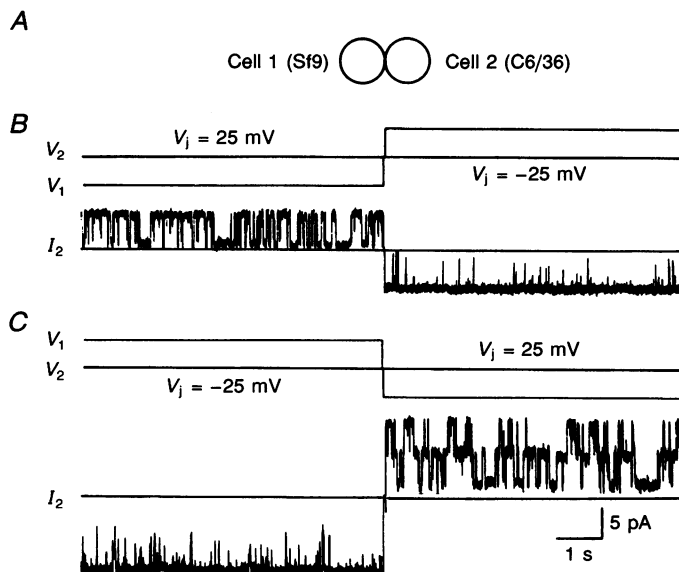
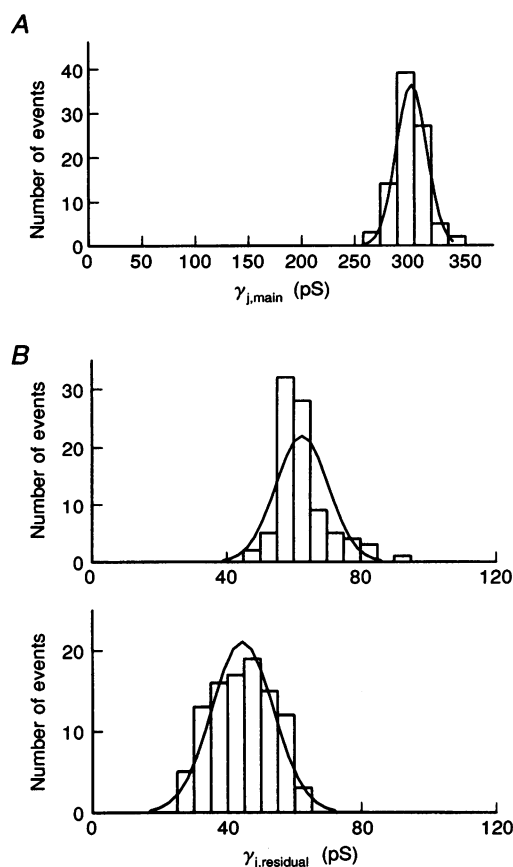


Figure 6. Activity of heterotypic channels depends on polarity of V_j

A, schematic representations of cell arrangement. Cell 1, Sf9; cell 2, C6/36. B, preparation with single channel. When the V_m of cell 2 was more positive than the V_m of cell 1 ($V_j = 25$ mV; left-hand side), the channel spent a similar time in the fully open state and residual state (upward deflections in I_2 : channel openings). When the V_m of cell 2 was more negative than the V_m of cell 1 ($V_j = -25$ mV; right-hand side), the channel spent most time in the fully open state (downward deflections in I_1 : channel openings). C, preparation with two channels. As in B, heterotypic channels are open more frequently at negative V_j ($V_j = -25$ mV; left-hand side) than at positive V_j ($V_j = 25$ mV; right-hand side).

Figure 7. Histograms of single-channel conductances of heterotypic channels (Sf9–C6/36) gained from 5 preparations

The continuous curves are the theoretical fit of data to a Gaussian distribution. *A*, histogram of $\gamma_{j,\text{main}}$ data. Individual values of $\gamma_{j,\text{main}}$ were pooled in 15 pS bins. Number of observations was plotted *versus* $\gamma_{j,\text{main}}$. The mean $\gamma_{j,\text{main}}$ was 303 ± 15 pS ($n = 89$). *B*, histograms of $\gamma_{j,\text{residual}}$ data obtained at positive V_j (upper panel) and negative V_j (lower panel). Bin size, 5 pS. Positive V_j (inside of C6/36 cell positive compared with Sf9 cell): $\gamma_{j,\text{residual}} = 64 \pm 10$ pS ($n = 75$). Negative V_j (inside of Sf9 cell positive compared with C6/36 cell): $\gamma_{j,\text{residual}} = 45 \pm 9$ pS ($n = 100$).



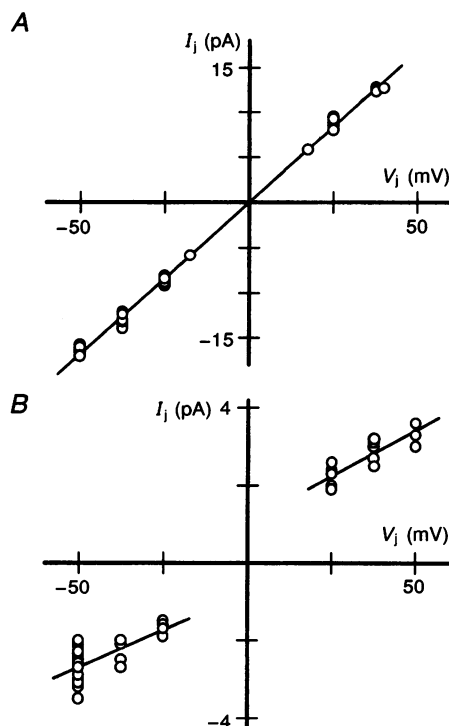
Conductances of heterotypic gap junction channels

Early during formation of a gap junction, each induced cell pair passed through a period with only one operational channel. The duration of this period varied from 1 to 8 min. This time window was used to determine the conductances

of heterotypic channels. Immediately after the first channel appearance, V_j was altered systematically up to ± 50 mV. The associated current records were analysed for discrete levels to determine the single-channel conductances. The values collected from five preparations were grouped into three data

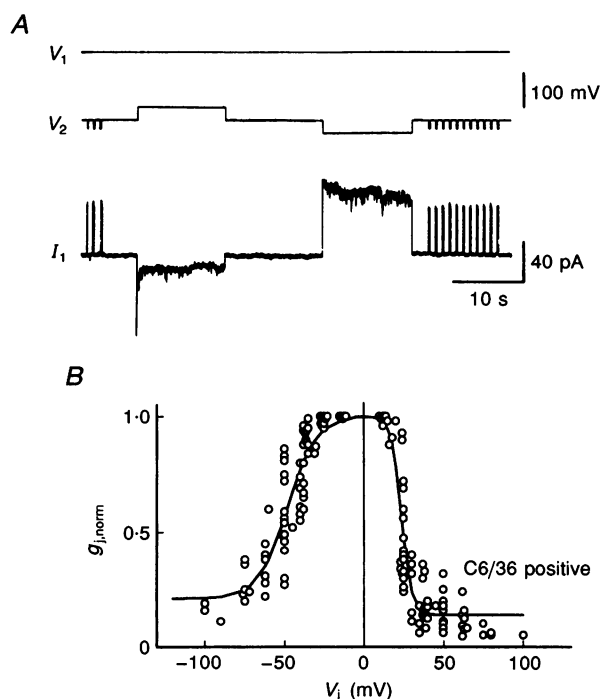
Figure 8. Current–voltage relationships of a heterotypic gap junction channel (Sf9–C6/36)

Amplitudes of $I_{j,\text{main}}$ and $I_{j,\text{residual}}$ were plotted *versus* V_j . *A*, $I_{j,\text{main}}$ data indicate that V_j polarity has no effect on $\gamma_{j,\text{main}}$. Linear regression analysis: slope = 0.340 pA mV^{-1} , equivalent to a conductance of 340 pS ($r = 0.99$; $n = 31$). *B*, $I_{j,\text{residual}}$ data indicate that V_j polarity and V_j amplitude have an effect on $\gamma_{j,\text{residual}}$. Linear regression analysis for negative V_j : slope = 0.038 pA mV^{-1} , corresponding to a conductance of 38 pS ($r = 0.77$; $n = 30$); values for positive V_j : slope = 0.047 pA mV^{-1} , corresponding to a conductance of 47 pS ($r = 0.88$; $n = 18$).



sets. In the case of $\gamma_{j,\text{main}}$, the values were sampled in 15 pS bins, but for $\gamma_{j,\text{residual}}$, the data for positive and negative V_j values were pooled separately and sampled in 5 pS bins. Figure 7 illustrates the resulting histograms plotting the number of observations *versus* γ_j . The analysis yielded the following mean values: $\gamma_{j,\text{main}} = 303 \pm 15$ pS ($n = 89$; Fig. 7A); for positive V_j values, $\gamma_{j,\text{residual}} = 64 \pm 10$ pS ($n = 88$; Fig. 7B, upper panel); for negative V_j values, $\gamma_{j,\text{residual}} = 45 \pm 9$ pS ($n = 98$; Fig. 7B, lower panel). These results are consistent with the view that the hemi-channels which form the Sf9–C6/36 channels have a different $\gamma_{j,\text{residual}}$, and that only one hemi-channel is involved at a time during V_j -dependent gating of a gap junction channel.

Figure 8 illustrates the current–voltage relationships of a heterotypic channel. The results were taken from a single experiment. The amplitudes of $I_{j,\text{main}}$ and $I_{j,\text{residual}}$ were plotted *versus* V_j . In the case of $I_{j,\text{main}}$ data (Fig. 8A), the linear regression analysis revealed a slope of 0.34 pA mV^{-1} (continuous line; regression coefficient (r) = 0.99 , $n = 31$) equivalent to a conductance of 340 pS. This implies that $\gamma_{j,\text{main}}$ is insensitive to V_j over the voltage range examined. In the case of $I_{j,\text{residual}}$ data (Fig. 8B), the graph showed more complex behaviour. There was a discontinuity at the origin giving rise to two different slopes. The linear regression analysis revealed the following data: for negative V_j values (inside of the Sf9 cell positive relative to the C6/36 cell), the slope was shallower (0.038 pA mV^{-1} ; $r = 0.77$, $n = 30$) and corresponded to a $\gamma_{j,\text{residual}}$ of 38 pS. For positive V_j values (inside of the C6/36 cell positive relative to the Sf9 cell), the slope was steeper (0.047 pA mV^{-1} ; $r = 0.88$, $n = 18$) and equalled a $\gamma_{j,\text{residual}}$ of 47 pS. This suggests that $\gamma_{j,\text{residual}}$ depends on the polarity of V_j and that the functions $\gamma_{j,\text{residual}} = f(V_j)$ do not go through the origin.



V_j dependency of heterotypic gap junctions

In conjunction with the induced cell pair approach, after successful insertion of the first gap junction channel, g_j continued to increase for 11–15 min. As a result, functionally stable gap junctions developed that were suitable for studying the V_j sensitivity of g_j . Figure 9 documents the dependency of I_j and g_j on V_j in Sf9–C6/36 cell pairs. Figure 9A shows the original records. In this case the Sf9 cell corresponds to cell 1 and the C6/36 cell to cell 2. The pulse protocol was identical to that in Fig. 1A (see Dependence of g_j on junctional potential). Depolarization of the C6/36 cell by 37.5 mV provoked an I_j with a pronounced time-dependent decay (trace I_j , left-hand side). Hyperpolarization of the C6/36 cell by the same amount generated an I_j with a marginal relaxation (trace I_j , right-hand side). This indicates that I_j is sensitive to the polarity of V_j with respect to time-dependent decay and steady-state amplitude. Figure 9B summarizes the collected results from six experiments. The amplitudes of $I_{j,\text{inst}}$ and $I_{j,\text{ss}}$ were measured and the conductances $g_{j,\text{inst}}$ and $g_{j,\text{ss}}$ determined. The normalized values of g_j ($g_{j,\text{norm}} = g_{j,\text{ss}}/g_{j,\text{inst}}$) were then plotted *versus* V_j . The graph documents that $g_{j,\text{norm}}$ did not show a symmetrical relationship with V_j . The continuous curve corresponds to the best fit of the data to the Boltzmann equation using the following parameters for negative and positive V_j , respectively: $V_{j,0} = -48.3$ and 23.5 mV, $g_{j,\text{min}} = 0.21$ and 0.14 , $z = 4.1$ and 18.7 .

V_m dependency of heterotypic gap junctions

Induced cell pairs with stable electrical coupling (many channels) were also used to examine the relationship $g_j = f(V_m)$ of Sf9–C6/36 gap junctions. Figure 10A shows records illustrating the dependency of I_j on V_m . V_1 and V_2 represent the membrane potential of the Sf9 cell and the

Figure 9. Gap junctions with heterotypic channels (Sf9–C6/36): dependence of g_j on V_j

Cell 1, Sf9; cell 2, C6/36. A, establishment of positive (left-hand side) or negative (right-hand side) V_j gradient of 37.5 mV (trace V_2) revealed an I_j with distinct time-dependent inactivation or weak inactivation, respectively (trace I_j). Short test pulses (25 mV, 200 ms, 1 Hz) were applied periodically to cell 2 to monitor the electrical stability of the preparation. $V_h = -70$ mV. B, plot of normalized gap junction conductance ($g_{j,\text{norm}}$) *versus* V_j . Data from 6 preparations. Negative V_j : C6/36 cell hyperpolarized; positive V_j : C6/36 cell depolarized. The continuous curve is the best fit of the data to the Boltzmann equation. Negative V_j : $V_{j,0} = -48.3$ mV, $g_{j,\text{min}} = 0.21$, $z = 4.1$; positive V_j : $V_{j,0} = 23.5$ mV, $g_{j,\text{min}} = 0.14$, $z = 18.7$.

C6/36 cell, respectively. The pulse protocol adopted was identical to that in Fig. 2A (see Dependence of g_j on membrane potential). In this case I_j was monitored following repetitive application of a hyperpolarizing test pulse to cell 2 to evoke a V_j (15 mV, 200 ms, 1 Hz). Starting from a common holding potential of -70 mV, depolarization of both cells to 55 mV (traces V_1 and V_2 , left-hand side) produced a time-dependent decrease in I_j (upward deflections in I_j). Return to the holding potential led to a recovery of I_j with time. Subsequent hyperpolarization of the cells to -95 mV (right-hand side) had virtually no effect on I_j . The records in Fig. 10A and others from the same experiment were used to determine g_j immediately before ($g_{j,\text{control}}$) and at the end of a conditioning pulse ($g_{j,\text{ss}}$). The normalized values ($g_{j,\text{norm}} = g_{j,\text{ss}}/g_{j,\text{control}}$) were then plotted versus V_m . Figure 10B summarizes the results from seven experiments. The data points follow a sigmoidal curve with $g_{j,\text{norm}}$ decreasing from unity to zero as V_m is depolarized. The continuous curve represents the best fit of the data to the Boltzmann equation using the following values: $V_{m,0} = 2$ mV, $g_{j,\text{min}} = 0$, $z = 2.9$.

DISCUSSION

Sf9 cells together with baculovirus vectors are often used for gene expression studies (Summers & Smith, 1987). However, it turned out that this system is not ideal to examine exogenous connexins. We found out that Sf9 cells form gap junctions and hence must possess an endogenous gap junction protein. Furthermore, we noticed that g_j was insensitive to V_j , V_m , and heptanol in some cell pairs. These cell-to-cell contacts presumably consist of cytoplasmic

bridges rather than gap junctions (Bukauskas *et al.* 1992a, b). Histologists have observed such structures in dividing cells (see Bukauskas *et al.* 1992b). Functional evidence for cytoplasmic bridges was provided for mammalian cell lines (HeLa: Bukauskas *et al.* 1995b; RIN: Banach & Weingart, 1996). Their existence questions the interpretation of a number of experiments aimed at identifying gap junctions. As discussed before (Bukauskas *et al.* 1992a, b), plane current flow or dye diffusion may not be sufficient to prove the presence of gap junctions. More stringent functional criteria are required.

Voltage gating of Sf9–Sf9 gap junctions

Our experiments with preformed cell pairs indicated that g_j is controlled by V_j and V_m . This is consistent with previous reports on other insect cells (salivary gland of *Chironomus thummi* and *Drosophila melanogaster*: Obaid *et al.* 1983, Verselis *et al.* 1991; C6/36 cells of *Aedes albopictus*: Bukauskas *et al.* 1992a; epidermal cells of *Tenebrio molitor*: Churchill & Caveney, 1993).

With respect to V_j dependence, we found that the g_j/V_j relationship at steady state is bell shaped and nearly symmetrical (see Fig. 1B). The data were best fitted by the Boltzmann equation with $V_{j,0}$ values of -54 and 55 mV, $g_{j,\text{min}}$ of 0.24 and 0.23 , and z of 5.5 and 6.1 for negative and positive V_j , respectively. These parameters are different from those reported for C6/36 cells ($V_{j,0} = -31$ and 24 mV; $g_{j,\text{min}} = 0.15$ and 0.14 ; $z = 2.7$ and 3.3 ; Weingart & Bukauskas, 1995), suggesting that Sf9 cells and C6/36 cells have different gap junction proteins. The gap junctions of the latter resemble those of epidermal cells of *Tenebrio*

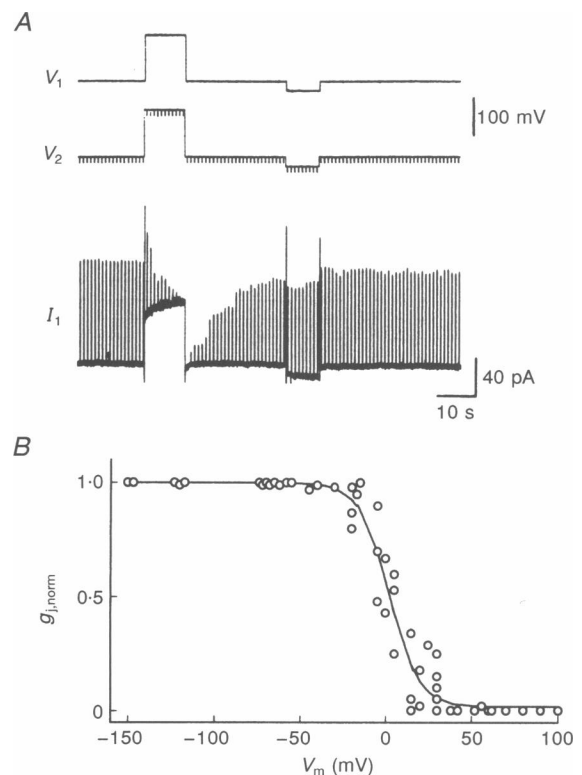


Figure 10. Gap junctions with heterotypic channels (Sf9–C6/36): dependence of g_j on V_m

A, records of V_1 , V_2 and I_1 corresponding to membrane potential of cell 1 (Sf9) and cell 2 (C6/36) and current of cell 1, respectively. A conditioning pulse was administered simultaneously to both cells, first in the depolarizing direction (125 mV; left-hand side) and then in the hyperpolarizing direction (25 mV; right-hand side), while test pulses were applied repetitively to cell 2 (15 mV, 200 ms, 1 Hz) to assay g_j . This gave rise to a time-dependent decrease in I_j and virtually no change in I_j (upward deflections in I_j).

$V_h = -70$ mV. B, plot of normalized g_j ($g_{j,\text{norm}}$) versus V_m . Data from 7 preparations. The continuous curve is the best fit of data to the Boltzmann equation with $V_{m,0} = 2$ mV, $g_{j,\text{min}} = 0$ mV and $z = 2.9$.

molitor (Fig. 6 in Churchill & Caveney, 1993: $V_{j,0} = 35$ mV, $g_{j,\min} = 0.18$). With respect to V_m dependence, our studies revealed a sigmoidal g_j/V_m relationship at steady state (see Fig. 2B). The value of g_j was maximal near the intrinsic V_m , i.e. approximately -50 mV. In contrast to V_j gating, V_m gating showed a complete inhibition of g_j at positive V_m values. The data were well fitted by the Boltzmann equation with values for $V_{m,0}$ and z of 13 mV and 1.5, respectively. These parameters are similar to those reported for C6/36 cells ($V_{m,0} = 10$ mV, $z = 2.8$; Weingart & Bukauskas, 1995). Thus, gap junctions of Sf9 cells and C6/36 cells cannot be distinguished on the basis of V_m gating. A comparison of the Boltzmann parameters indicates that the gap junctions of these cells are similar to those of *Drosophila* salivary glands ($V_{m,0} = 5$ mV, $z = 2.1$; Verselis *et al.* 1991), but different from those of *Tenebrio* epidermal cells ($V_{m,0} = -5.5$ mV, $z = 1.5$; Churchill & Caveney, 1993) and *Chironomus* salivary glands ($V_{m,0} = -27$ mV, $z = 2$; Obaid *et al.* 1983).

In conclusion, voltage gating predicts the existence of several insect gap junction proteins. This family of proteins may comprise at least two (possibly four) different members.

Properties of Sf9–Sf9 channels

Sf9–Sf9 channels have several conductance states. The most prominent states are $\gamma_{j,\text{main}}$ and $\gamma_{j,\text{residual}}$. On rare occasions, i.e. at intermediate V_j values and early during pulses, we observed substate conductances ($\gamma_{j,\text{substates}}$) interposed between $\gamma_{j,\text{main}}$ and $\gamma_{j,\text{residual}}$ (not shown). When both cells were depolarized, the channels went into yet another state – a closed state ($\gamma_{j,\text{closed}}$; not shown). Current transitions between open states (i.e. main state, substates, residual state) were fast (< 2 ms; see Fig. 3) while those involving the closed state were slow (tens of milliseconds; not shown). Thus, like C6/36–C6/36 channels (Bukauskas & Weingart, 1994a), Sf9–Sf9 channels possess two voltage-sensitive gates, a V_j gate and a V_m gate.

The analysis of the Sf9–Sf9 channels yielded $\gamma_{j,\text{main}}$ and $\gamma_{j,\text{residual}}$ conductances of 224 and 42 pS, respectively. The related values for C6/36 cells were 375 and 30–90 pS, respectively (Bukauskas & Weingart, 1994a). In the case of C6/36 cells, $\gamma_{j,\text{residual}}$ was sensitive to V_j . If present at all, this property was weak in Sf9 cells (not shown). These data support the view that the two types of cells express different gap junction proteins. For comparison, insect haemocytes (cockroach *Periplaneta*; Churchill, Coodin, Shivers & Caveney, 1993) and annelida giant axons (earthworm *Lumbricus*; Brink & Fan, 1989) exhibit a γ_j of 325 and 100 pS, respectively. These values presumably correspond to differences between $\gamma_{j,\text{main}}$ and $\gamma_{j,\text{residual}}$, not to $\gamma_{j,\text{main}}$ (see Bukauskas & Weingart, 1994a).

The existence of $\gamma_{j,\text{residual}}$ suggests that the incomplete inactivation of $g_{j,\text{ss}}$ at large V_j values (see Fig. 1B) is caused by a partial channel closure rather than a residual open channel probability. The similarity of the ratios $g_{j,\text{inst}}/g_{j,\text{ss}} = 4.1$ and $\gamma_{j,\text{main}}/\gamma_{j,\text{residual}} = 5.3$ supports this

view. A $\gamma_{j,\text{residual}}$ has also been established for vertebrate channels (Cx26, Cx32: Bukauskas *et al.* 1995a; Cx40: Bukauskas *et al.* 1995b; Cx43: Valiunas, Bukauskas & Weingart, 1995). It may be a genuine property of gap junction channels and it may provide a means to modulate intercellular signalling. The presence of $\gamma_{j,\text{closed}}$ and the subsequent arrest of fast channel activity offer an explanation for the complete decline of $g_{j,\text{ss}}$ at positive V_m values (see Fig. 2B). This behaviour was also observed in C6/36–C6/36 channels (Bukauskas & Weingart, 1994a).

In summary, the single-channel data suggest the existence of several insect gap junction proteins. Most relevant for this study, gap junction channels of Sf9 cells and C6/36 cells exhibit different properties.

Formation of heterotypic Sf9–C6/36 channels

De novo formation of gap junction channels can be caused by forcing two cells into physical contact. We have used this approach with C6/36 cells (Bukauskas & Weingart, 1994a), neonatal rat heart cells (Valiunas *et al.* 1995) and transfected HeLa cells (Bukauskas & Weingart, 1995; Bukauskas *et al.* 1995a,b). Here we show that it is also useful to study heterotypic channels between Sf9 cells and C6/36 cells. The first sign of a newly formed channel was observed ~ 13 min after cell-to-cell contact. The process of channel insertion continued thereafter. After 15 min, g_j had reached a value of 2.1 nS corresponding to seven channels (assuming that $\gamma_{j,\text{main}} = 303$ pS; see Properties of heterotypic Sf9–C6/36 channels). These findings are consistent with the view that the cell membranes contain precursors of gap junctions, i.e. hemi-channels (Dahl, Werner, Levine & Rabadan-Diehl, 1992) and that gap junction proteins have extracellular loops with compatible docking domains.

The mechanism of channel formation is largely unknown. It may involve the recognition of extracellular sites and anchorage by adhesion molecules (Meyer, Laird, Revel & Johnson, 1992) followed by lateral diffusion of hemi-channels, docking of hemi-channels and recruitment of channels. The nature of the forces responsible for the integrity of gap junction channels is also unclear.

Properties of heterotypic Sf9–C6/36 channels

Gap junction channels consist of two hemi-channels (hc1 and hc2) arranged in series. Their conductance can be expressed as:

$$\gamma_j = (\gamma_{j(\text{hc1})}\gamma_{j(\text{hc2})})/(\gamma_{j(\text{hc1})} + \gamma_{j(\text{hc2})}). \quad (2)$$

This equation allows some predictions: for example, when $\gamma_{j(\text{hc1})}$ and $\gamma_{j(\text{hc2})}$ are comparable, both hemi-channels contribute equally to the channel conductance. This condition exists at the main state (small V_j) of homotypic channels and of heterotypic channels with hemi-channels of similar conductance. Alternatively, when $\gamma_{j(\text{hc1})}$ and $\gamma_{j(\text{hc2})}$ are largely different, γ_j is determined primarily by the low conductance hemi-channel. This situation prevails at the main state of heterotypic channels with hemi-channels of disparate

conductance. It is also relevant for channels in the residual state (large V_j) with one hemi-channel in the residual state and one in the main state. These considerations set the framework for a discussion on heterotypic channels.

The I_j records indicate that Sf9–C6/36 channels exhibit complex properties. The analysis revealed a linear relationship for $I_{j,\text{main}} = f(V_j)$ (range examined, ± 50 mV) and a $\gamma_{j,\text{main}}$ of 303 pS. This value of $\gamma_{j,\text{main}}$ is slightly larger than that predicted from the series arrangement of a Sf9 and a C6/36 hemi-channel, i.e. $(448 \times 750)/(448 + 750) = 280$ pS. The discrepancy could be due to channel deformation during docking. Heterotypic docking may lead to shorter channels or channels with larger cross sections when compared with homotypic docking. In contrast to the main state, the residual state of Sf9–C6/36 channels depends on the polarity of V_j . This is documented by the two histograms in Fig. 7B: $\gamma_{j,\text{residual}}$ was 45 pS for negative V_j values (Sf9 cell inside positive; see lower panel) and 64 pS for positive V_j values (C6/36 cell inside positive; see upper panel). This property is also reflected in the shallower slope of the function $I_{j,\text{residual}} = f(V_j)$ for negative V_j values (see Fig. 8B). The analyses in Fig. 8B also indicate that the relationships $I_{j,\text{residual}} = f(V_j)$ for negative and positive V_j values do not go through the origin. This observation suggests that gap junction channels switch from one hemi-channel to the other when the polarity of V_j is inverted. Our mathematical model for gap junction channels of vertebrates anticipates this behaviour (Weingart *et al.* 1996; R. Vogel & R. Weingart, unpublished observations).

These observations are compatible with the notion that each hemi-channel has a separate V_j gate. For negative V_j values, Sf9–C6/36 channels exhibit a $\gamma_{j,\text{residual}}$ which resembles the

$\gamma_{j,\text{residual}}$ of homotypic Sf9 channels (45 versus 42 pS). For positive V_j values, these channels show a $\gamma_{j,\text{residual}}$ which is similar to the $\gamma_{j,\text{residual}}$ of homotypic C6/36 channels (64 versus 65 pS; the latter corresponds to the mean $\gamma_{j,\text{residual}}$ reported by Bukauskas & Weingart, 1994a). This suggests that in both types of hemi-channels the V_j gate closes when the cytoplasmic aspect is made positive. As a result, a fast transition occurs between the main state and the residual state.

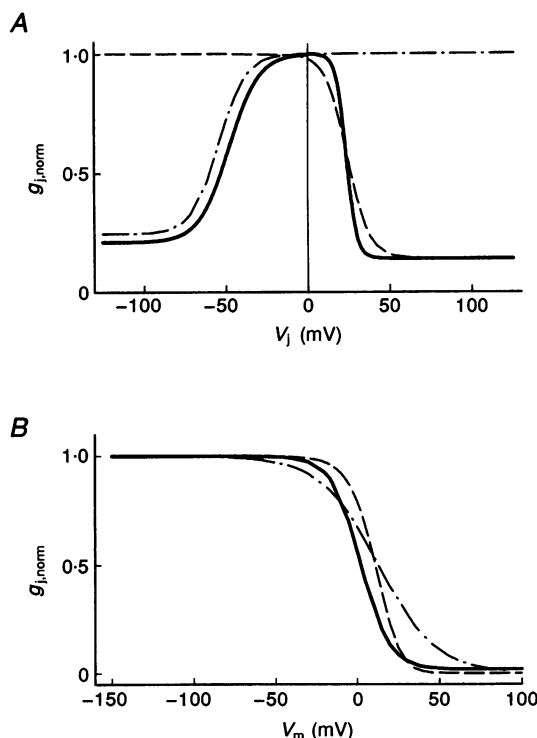
The residual conductance of Sf9–C6/36 channels can also be predicted from the homotypic channel data by means of eqn (2). The series arrangement of a C6/36 hemi-channel in the residual state ($\gamma_{j(\text{hcl})} = 71$ pS, calculated from $\gamma_{j,\text{residual}} = 65$ pS; Bukauskas & Weingart, 1994a) and a Sf9 hemi-channel in the main state ($\gamma_{j(\text{hcl})} = 448$ pS; this paper) leads to a $\gamma_{j,\text{residual}}$ of 61 pS. The series arrangement of a Sf9 hemi-channel in the residual state ($\gamma_{j(\text{hcl})} = 46$ pS; this paper) and a C6/36 hemi-channel in the main state ($\gamma_{j(\text{hcl})} = 750$ pS; Bukauskas & Weingart, 1994a) gives a $\gamma_{j,\text{residual}}$ of 44 pS. Thus, the calculated and measured values of $\gamma_{j,\text{residual}}$ are close (61 and 44 pS versus 64 and 45 pS). Finally, we have found that Sf9–C6/36 channels exhibit substates (not shown). In this respect they also behave like homotypic channels of Sf9 cells or C6/36 cells.

Voltage gating of heterotypic Sf9–C6/36 gap junctions

Sf9–C6/36 gap junctions show a moderate V_j -dependent rectification. Hyperpolarization of the C6/36 cell (negative V_j) gave rise to a larger $I_{j,\text{ss}}$ than depolarization (positive V_j ; see Fig. 9A). This resulted in an asymmetric relationship $g_{j,\text{norm}} = f(V_j)$ (see Fig. 9B). For negative and positive V_j values, the $g_{j,\text{norm}}$ data resemble those of homotypic Sf9 and

Figure 11. Comparison of homotypic and heterotypic insect gap junctions

A, relationship between normalized gap junction conductance at steady state ($g_{j,\text{norm}}$) and gap junction potential (V_j).
B, relationship between $g_{j,\text{norm}}$ and membrane potential (V_m).
Continuous curves show the heterotypic gap junction Sf9–C6/36, dotted and dashed lines show the homotypic gap junction Sf9–Sf9 and the dashed line shows the homotypic gap junction C6/36–C6/36. For parameters, see text.



C6/36 gap junctions, respectively (see Fig. 11A). A comparison of the Boltzmann parameters reinforces this conclusion (Sf9: $V_{j,0} = -54$ mV, $g_{j,\min} = 0.24$, $z = 5.5$ for negative V_j values (this paper); C6/36: $V_{j,0} = 24$ mV, $g_{j,\min} = 0.14$, $z = 3.3$ for positive V_j values (Weingart & Bukauskas, 1995); Sf9–C6/36: $V_{j,0} = -48$ and 23.5 mV, $g_{j,\min} = 0.21$ and 0.14 , $z = 4.1$ and 18.7 for negative and positive V_j values (this paper)). These data are consistent with the view that positivity at the cytoplasmic aspect of Sf9 hemi-channels or C6/36 hemi-channels provokes closure of the V_j gate. However, the fit between homotypic and heterotypic data is not perfect. At negative V_j values, $V_{j,0}$ was more negative in heterotypic gap junctions. At positive V_j values, z was larger in heterotypic gap junctions. This suggests that docking of hemi-channels may affect channel gating.

Similar properties of heterotypic gap junctions have been reported for vertebrate connexins using the oocyte expression system or transfected cells (Swenson, Jordan, Beyer & Paul, 1989; Werner *et al.* 1989; Barrio *et al.* 1991; Rubin *et al.* 1992; Nicholson *et al.* 1993). These studies suggest that connexon gating is caused by positive V_j values (but see Verselis, Ginter & Bargiello, 1994).

Sf9–C6/36 gap junctions display a sigmoidal relationship, $g_{j,\text{norm}} = f(V_m)$, with the Boltzmann parameters of $V_{m,0} = 2$ mV, $g_{j,\min} = 0$ and $z = 2.9$ (see Fig. 10A). A simple scheme predicts that the values for $V_{m,0}$ and z are intermediate to those of homotypic gap junctions. However, Fig. 11B shows that this is not the case. The function $g_{j,\text{norm}} = f(V_m)$ is shifted along the V_m axis when compared with that of homotypic gap junctions (Sf9: $V_{m,0} = 13$ mV, this paper; C6/36: $V_{m,0} = 10$ mV, Weingart & Bukauskas, 1995). Furthermore, z is larger in Sf9–C6/36 gap junctions than in Sf9–Sf9 gap junctions ($z = 1.5$; this paper), but close to that in C6/36–C6/36 gap junctions ($z = 2.8$; Weingart & Bukauskas, 1995). This suggests that the docking of hemi-channels is involved in determining the properties of V_m -sensitive gating.

To interpret our data we assumed that both Sf9 cells and C6/36 cells express a single type of gap junction protein. This assumption was based on microscopic and macroscopic currents. The rationale was that co-expression of more than one type of channel with different properties would lead to a broad spectrum of data for C6/36–C6/36 and Sf9–Sf9 cell pairs. Yet we observed narrow histograms for $\gamma_{j,\text{main}}$ and homogeneous relationships for $g_{j,\text{norm}} = f(V_j)$ and $g_{j,\text{norm}} = f(V_m)$ (Bukauskas & Weingart, 1994a; Weingart & Bukauskas, 1995; this paper). However, we cannot exclude the possibility that these cells co-express several gap junction proteins of similar properties.

- BANACH, K. & WEINGART, R. (1996). Connexin43 gap junctions exhibit asymmetrical gating properties. *Pflügers Archiv* **431**, 775–785.
- BARNES, T. M. (1994). OPUS: a growing family of gap junction proteins? *Trends in Genetics* **10**, 303–305.
- BARRIO, L. C., SUCHYNA, T., BARGIELLO, T. A., XIAN HU, L., ROGINSKI, R., BENNETT, M. V. L. & NICHOLSON, B. (1991). Gap junctions formed by connexin 26 and 32 alone and in combination are differently affected by applied voltage. *Proceedings of the National Academy of Sciences of the USA* **88**, 8410–8414.
- BENNETT, M. V. L., BARRIO, L. C., BARGIELLO, T. A., SPRAY, D. C., HERTZBERG, E. & SAEZ, J. C. (1991). Gap junctions: new tools, new answers, new questions. *Neuron* **6**, 305–320.
- BERDAN, R. C. & GILULA, N. B. (1988). The arthropod gap junction and pseudo-gap junction: Isolation and preliminary biochemical analysis. *Cell and Tissue Research* **251**, 257–274.
- BEYER, E. C. (1993). Gap junctions. *International Review of Cytology* **137C**, 1–37.
- BRINK, P. R. & FAN, S. (1989). Patch clamp recordings from membranes which contain gap junction channels. *Biophysical Journal* **56**, 579–593.
- BUKAUSKAS, F. F., ELFGANG, C., WILLECKE, K. & WEINGART, R. (1995a). Heterotypic gap junction channels (connexin 26–connexin 32) violate the paradigm of unitary conductance. *Pflügers Archiv* **429**, 870–872.
- BUKAUSKAS, F. F., ELFGANG, C., WILLECKE, K. & WEINGART, R. (1995b). Biophysical properties of gap junction channels formed by mouse connexin 40 in induced pairs of transfected human HeLa cells. *Biophysical Journal* **68**, 2289–2298.
- BUKAUSKAS, F., KEMPF, C. & WEINGART, R. (1992a). Electrical coupling between cells of the insect *Aedes albopictus*. *Journal of Physiology* **448**, 321–337.
- BUKAUSKAS, F. F., KEMPF, C. & WEINGART, R. (1992b). Cytoplasmic bridges and gap junctions in an insect cell line (*Aedes albopictus*). *Experimental Physiology* **77**, 903–911.
- BUKAUSKAS, F. F. & WEINGART, R. (1994a). Voltage-dependent gating of single gap junction channels in an insect cell line. *Biophysical Journal* **67**, 613–625.
- BUKAUSKAS, F. F. & WEINGART, R. (1994b). Electrical properties of homotypic and heterotypic gap junctions between insect cells. *Experientia* **50**, A39.
- BUKAUSKAS, F. F. & WEINGART, R. (1995). Gating properties of homo- and heterotypic gap junction channels formed by different mouse connexins. *Proceedings of the 1995 Gap Junction Conference*, L'Île des Embiez, France.
- CHURCHILL, D. & CAVENEY, S. (1993). Double whole-cell patch-clamp characterization of gap junctional channels in isolated insect epidermal cell pairs. *Journal of Membrane Biology* **135**, 165–180.
- CHURCHILL, D., COODIN, S., SHIVERS, R. S. & CAVENEY, S. (1993). Rapid de novo formation of gap junctions between insect hemocytes *in vitro*: a freeze-fracture, dye-transfer and patch-clamp study. *Journal of Cell Sciences* **104**, 763–772.
- DAHL, G., WERNER, R., LEVINE, E. & RABADAN-DIEHL, C. (1992). Mutational analysis of gap junction formation. *Biophysical Journal* **62**, 172–182.
- IGARASHI, A. (1978). Isolation of a Singh's *Aedes albopictus* cell clone sensitive to Dengue and Chikungunya viruses. *Journal of General Virology* **40**, 531–544.

- MEYER, R. A., LAIRD, D. W., REVEL, J. P. & JOHNSON, R. G. (1992). Inhibition of gap junction and adherence junction assembly by connexin and A-CAM antibodies. *Journal of Cell Biology* **119**, 179–189.
- MORENO, A., FISHMAN, G. I., BEYER, E. C. & SPRAY, D. C. (1995). Voltage dependent gating and single channel analysis of heterotypic gap junction channels formed of Cx45 and Cx43. In *Intercellular Communication Through Gap Junctions: Progress in Cell Research*, vol. 4, ed. KANNO, Y., KATAOKA, K., SHIBA, Y., SHIBATA, Y. & SHIMAZU, T., pp. 405–408. Elsevier, Amsterdam.
- NICHOLSON, B. J., SUCHYNA, T., XU, L. X., HAMMERNICK, P., CAO, F. L., FOURTNER, C., BARRIO, L. & BENNETT, M. V. L. (1993). Divergent properties of different connexins expressed in *Xenopus* oocytes. In *Gap Junctions: Progress in Cell Research*, vol. 3, ed. HALL, J. E., ZAMPIGHI, G. A. & DAVIS, R. M., pp. 3–13. Elsevier, Amsterdam.
- OBAID, A. L., SOCOLAR, S. J. & ROSE, B. (1983). Cell-to-cell channels with two independently regulated gates in series: Analysis of junctional conductance modulation by membrane potential, calcium, and pH. *Journal of Membrane Biology* **73**, 69–89.
- RUBIN, J. B., VERSELIS, V. K., BENNETT, M. V. L. & BARGIELLO, T. A. (1992). Molecular analysis of voltage dependence of heterotypic gap junctions formed by connexins 26 and 32. *Biophysical Journal* **62**, 183–195.
- SMITH, G. E., JU, G., ERICSON, B. L., MOSCHERA, J., LAHM, H., CHIZZONITI, R. & SUMMERS, M. D. (1985). Modification and secretion of human interleukin 2 produced in insect cells by a baculovirus expression vector. *Proceedings of the National Academy of Sciences of the USA* **82**, 8404–8408.
- SUMMERS, M. D. & SMITH, G. E. (1987). A manual of methods for baculovirus vectors and insect cell culture procedures. Texas Agricultural Experimentation Station Bulletin, No. 1555.
- SWENSON, K. I., JORDAN, J. R., BEYER, E. C. & PAUL, D. L. (1989). Formation of gap junctions by expression of connexins in *Xenopus* oocyte pairs. *Cell* **57**, 145–155.
- VALIUNAS, V., BUKAUSKAS, F. F. & WEINGART, R. (1995). Neonatal rat heart cells: electrical gating of gap junction channels. *Experientia* **51**, A68.
- VERSELIS, V. K., BENNETT, M. V. L. & BARGIELLO, T. A. (1991). A voltage-dependent gap junction in *Drosophila melanogaster*. *Biophysical Journal* **59**, 114–126.
- VERSELIS, V. K., GINTER, C. S. & BARGIELLO, T. A. (1994). Opposite voltage gating polarities of two closely related connexins. *Nature* **368**, 348–351.
- WALTZMAN, M. N. & SPRAY, D. C. (1995). Exogenous expression of connexins for physiological characterization of channel properties: Comparison of methods and results. In *Intercellular Communication Through Gap Junctions: Progress in Cell Research*, vol. 4, ed. KANNO, Y., KATAOKA, K., SHIBA, Y., SHIBATA, Y., SHIMAZU, T., pp. 9–17. Elsevier, Amsterdam.
- WEINGART, R. & BUKAUSKAS, F. F. (1995). Gating properties of gap junction channels of an insect cell line. In *Intercellular Communication Through Gap Junctions: Progress in Cell Research*, vol. 4, ed. KANNO, Y., KATAOKA, K., SHIBA, Y., SHIBATA, Y., SHIMAZU, T., pp. 431–435. Elsevier, Amsterdam.
- WEINGART, R., BUKAUSKAS, F. F., VALIUNAS, V., VOGEL, R., WILLECKE, K. & ELFGANG, C. (1996). Heterotypic gap junctions and gating properties. In *Proceedings of Keystone Conference: Molecular Aspects to the Function of Intercellular Junctions*, p. 16.
- WERNER, R., LEVINE, E., RABADAN-DIEHL, C. & DAHL, G. (1989). Formation of hybrid cell–cell channels. *Proceedings of the National Academy of Sciences of the USA* **86**, 5380–5384.
- WHITE, T. W., BRUZZONE, R., WOLFRAM, S., PAUL, D. L. & GOODENOUGH, D. A. (1993). Selective interactions among the multiple connexin proteins expressed in the vertebrate lens: the second extracellular domain is a determinant of compatibility between connexins. *Journal of Cell Biology* **125**, 879–892.

Acknowledgements

The authors are indebted to Dr C. Kempf for providing the C6/36 cells and to Marlis Herrenschwand for expert technical assistance. This work was supported by the Swiss National Science Foundation (grants 31-36046.92 and 31-45554.95) and the Hochschulstiftung der Universität Bern.

Author's present address

F. K. Bukauskas: Department of Physiology, University of Rochester, 575 Elmwood Avenue, Rochester, NY 14642–8642, USA.

Author's email address

R. Weingart: weingart@pyl.unibe.ch

Received 19 August 1996; accepted 13 December 1996.